

Supplementary Materials

New insights into the formation of ammonium nitrate from a physical and chemical level perspective

Yuting Wei^{1,2}, Xiao Tian^{1,2}, Junbo Huang^{1,2}, Zaihua Wang (✉)³, Bo Huang⁴, Jinxing Liu^{5,6}, Jie Gao^{1,2}, Danni Liang^{1,2}, Haofei Yu⁷, Yinchang Feng^{1,2}, Guoliang Shi (✉)^{1,2}

1 State Environmental Protection Key Laboratory of Urban Ambient Air Particulate Matter Pollution Prevention and Control, Tianjin Key Laboratory of Urban Transport Emission Research, College of Environmental Science and Engineering, Nankai University, Tianjin 300350, China

2 CMA-NKU Cooperative Laboratory for Atmospheric Environment-Health Research (CLAER), College of Environmental Science and Engineering, Nankai University, Tianjin 300350, China

3 Institute of Resources Utilization and Rare Earth Development, Guangdong Academy of Sciences, Guangzhou 510650, China

4 Guangzhou Hexin Instrument Co., Ltd, Guangzhou 510530, China

5 State Key Laboratory of Precision Measuring Technology and Instruments, Tianjin Key Laboratory of air pollutants Monitoring Technology, School of Precision Instrument and Optoelectronics Engineering, Tianjin University, Tianjin 300072, China

6 Gigantic Technology (Tianjin) Co., Ltd, Tianjin 300384, China

7 Department of Civil, Environmental and Construction Engineering, University of Central Florida, FL32816, USA

✉Corresponding authors

E-mails: zaihuawang@163.com (Z. Wang); nksgl@nankai.edu.cn (G. Shi)

Text S1 The comparison between theoretical $\varepsilon(\text{NO}_3^-)$ and observed $\varepsilon(\text{NO}_3^-)$ ($\varepsilon(\text{NO}_3^-)_{\text{obs}}$)

In order to consider the influence of non-ideality, we made the comparison between theoretical $\varepsilon(\text{NO}_3^-)$ ($\varepsilon^*(\text{NO}_3^-)$) and observed $\varepsilon(\text{NO}_3^-)$ ($\varepsilon(\text{NO}_3^-)_{\text{obs}}$), the result was presented in Fig. S4. A poor correlation between $\varepsilon^*(\text{NO}_3^-)$ and $\varepsilon(\text{NO}_3^-)_{\text{obs}}$ was observed (Fig. S4(a)). Since $\varepsilon^*(\text{NO}_3^-)$ represents the result under ideal conditions, it may be quite different from the actual atmospheric environment. For this reason, the activity coefficient of nitrate is incorporated into the calculation formula of $\varepsilon^*(\text{NO}_3^-)$ to obtain the $\varepsilon^*(\text{NO}_3^-)$ under the non-ideal state, and mark it as $\varepsilon^*(\text{NO}_3^-)_{\text{ni}}$ for the convenience of distinguishing. It can be seen from Fig. S4(b) that the correlation between $\varepsilon^*(\text{NO}_3^-)$ and $\varepsilon(\text{NO}_3^-)_{\text{obs}}$ has only slightly improved. The possible reason is that there are many other species as well as physical and chemical processes in the environment that may affect the partitioning of nitrate, which cannot be simply quantified by mathematical formulas. The above results indicated non-ideality played a role in nitrate partitioning.

Text S2 Identification of reverse S-curve based on $\varepsilon^*(\text{NO}_3^-)_{\text{ni}}$

Given by the effect of non-ideality, we use $\varepsilon^*(\text{NO}_3^-)_{\text{ni}}$ as an indicator to identify the reverse S-curve, and the results were shown in [Fig. S5 and S6](#). It can be found that when $\varepsilon^*(\text{NO}_3^-)_{\text{ni}}$ was high in summer, there was an obvious reverse S-curve, while not obvious in spring ([Fig.S5](#)). A Boltzmann equation was applied to fit a regression curve for $\text{pH}-\varepsilon(\text{NH}_4^+)$ for summer samples with $\varepsilon^*(\text{NO}_3^-)_{\text{ni}} > 0.9$ and $\text{pH} < 5.5$. The R^2 was 0.37, which did not suggest a great reverse S-curve relationship. As the range of $\varepsilon^*(\text{NO}_3^-)_{\text{ni}}$ increased to more than 0.99, the regression curve for $\text{pH}-\varepsilon(\text{NH}_4^+)$ was re-fitted, and R^2 was 0.68. The improvement of R^2 indicates that the reverse S-curve relationship was better. While it can be found that $\varepsilon^*(\text{NO}_3^-)$ is the indicator for reverse S-curve capture and was greater than 0.8, R^2 can reach 0.97 ([Fig. 2\(b\)](#)), which showed a very good reverse S-curve relationship between pH and $\varepsilon(\text{NH}_4^+)$. By comparison, $\varepsilon^*(\text{NO}_3^-)$ is more suitable as an indicator to identify reverse S-curve in the actual atmospheric environment.

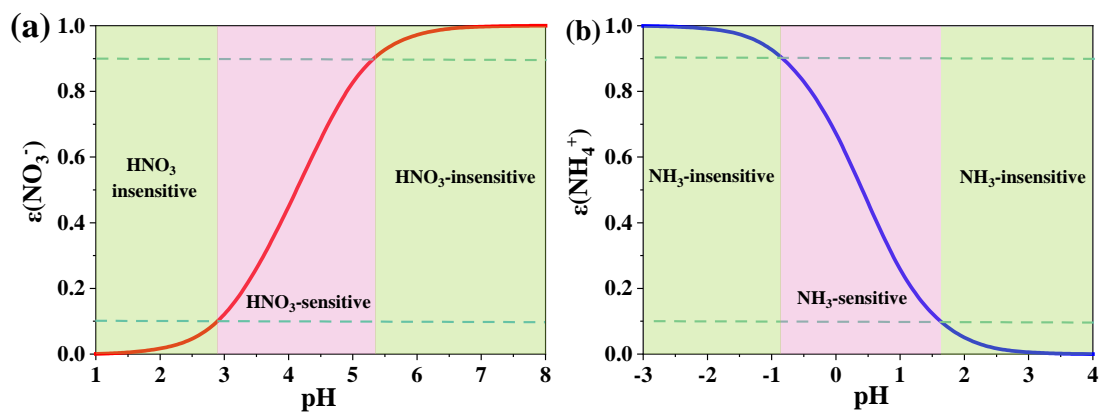


Fig. S1. Ideal S-curve and reverse S-curve of the equilibrium fraction of total nitrate in the aqueous phase. Relationship derived based on temperature of 295K and aerosol liquid water content of $1 \mu\text{g m}^{-3}$. We define the pH corresponding to the partitioning fraction of 10% to 90% as the position that defines whether the aerosol is sensitive to changes in gaseous precursors. ($\epsilon(\text{NO}_3^-) = [\text{NO}_3^-]/[\text{HNO}_3] + [\text{NO}_3^-]$, $\epsilon(\text{NH}_4^+) = [\text{NH}_4^+]/[\text{NH}_3] + [\text{NH}_4^+]$)

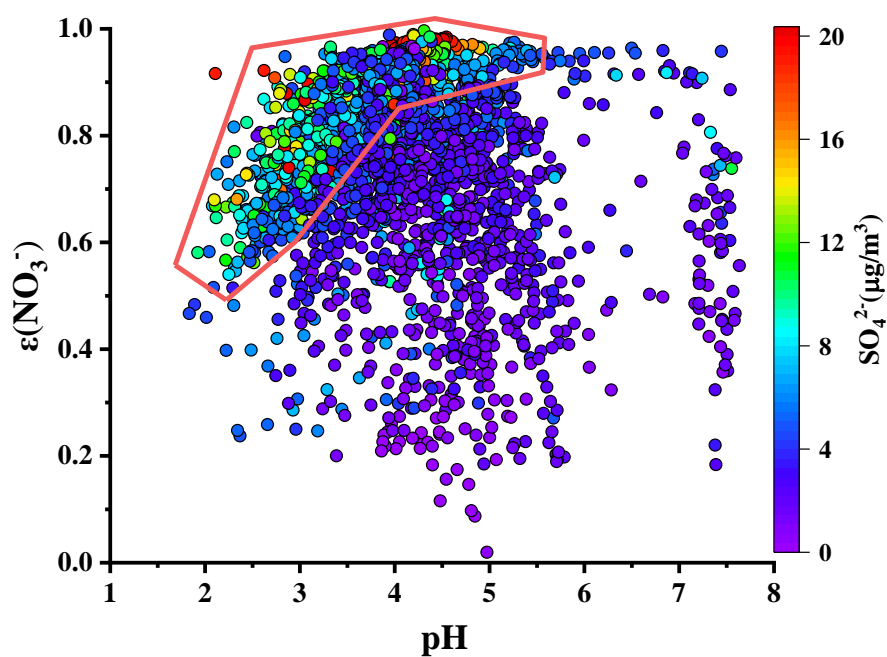


Fig. S2. $\epsilon(\text{NO}_3^-)$ as a function of pH for all samples. The color of the circles corresponds to observed secondary sulfate concentrations. Points with the red polygon are samples with higher concentrations of secondary sulfates.

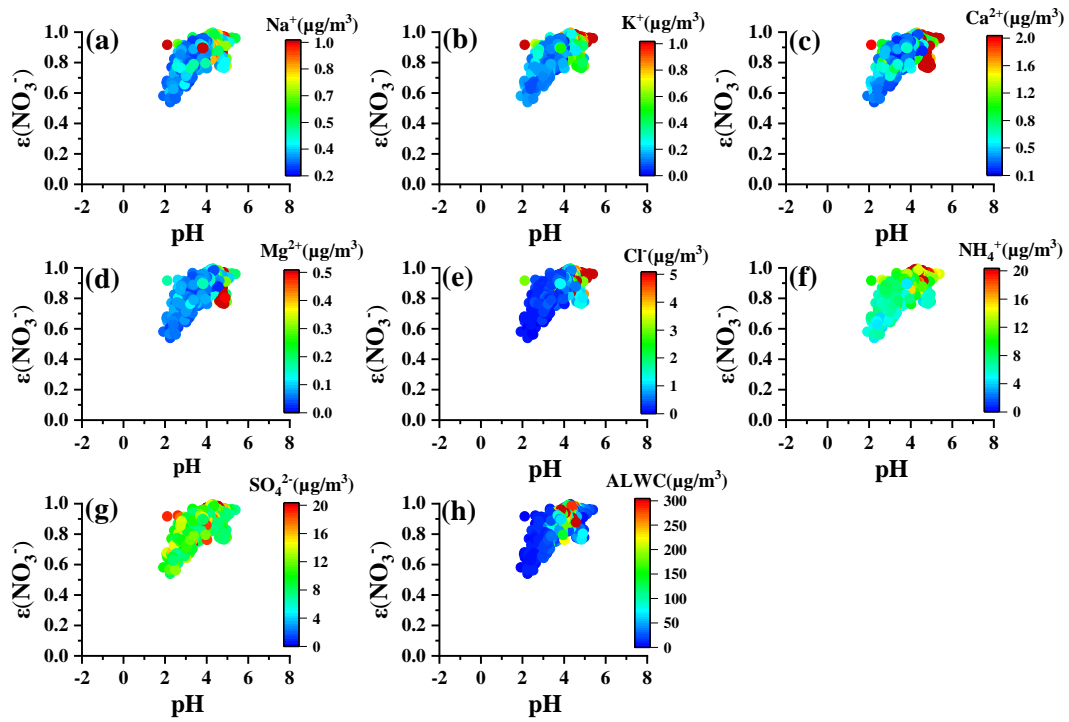


Fig. S3. $\varepsilon(\text{NO}_3^-)$ as a function of pH for all samples. The color of circles represents observed concentrations of (a) Na^+ , (b) K^+ , (c) Ca^{2+} , (d) Mg^{2+} , (e) Cl^- , (f) NH_4^+ , (g) SO_4^{2-} , and (h) aerosol liquid water content (ALWC)

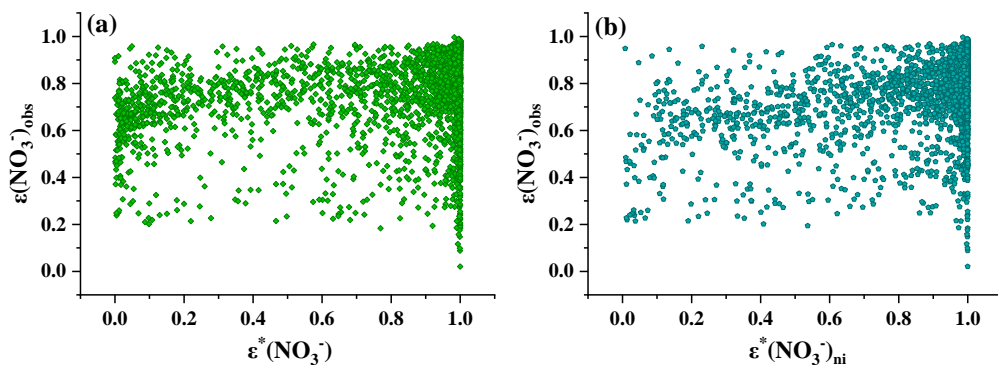


Fig. S4. The comparison of $\varepsilon^*(\text{NO}_3^-)$, $\varepsilon(\text{NO}_3^-)_{\text{obs}}$ and $\varepsilon^*(\text{NO}_3^-)_{\text{ni}}$

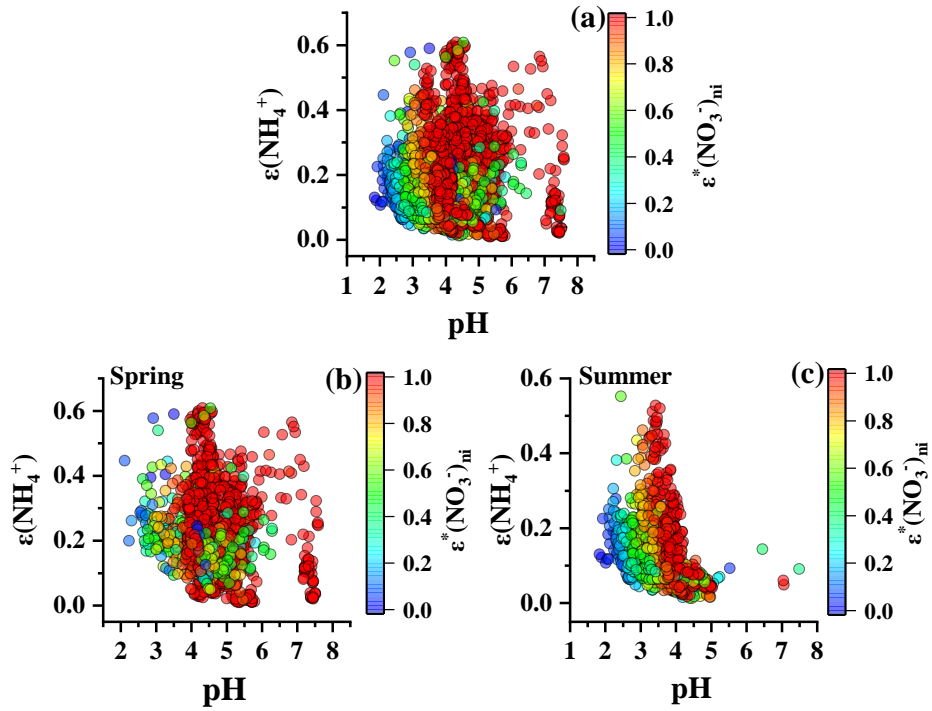


Fig. S5. $\epsilon(\text{NH}_4^+)$ as a function of pH for (a) all samples, (b) samples in spring, (c) samples in summer. Colors corresponds to $\epsilon^*(\text{NO}_3^-)_{\text{mi}}$ value

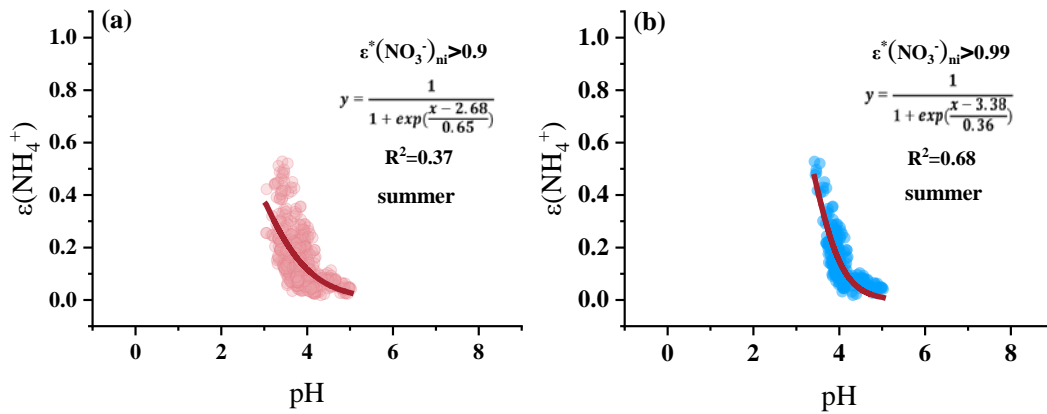


Fig. S6. Reverse S-curve constructed by fitting $\epsilon(\text{NH}_4^+)$ as a function of pH using the Boltzmann equation. (a)

Red points are actual atmospheric samples with $\epsilon^*(\text{NO}_3^-)_{\text{mi}}$ higher than 0.9 in summer. (b) Blue points are actual atmospheric samples with $\epsilon^*(\text{NO}_3^-)_{\text{mi}}$ higher than 0.99 in summer.

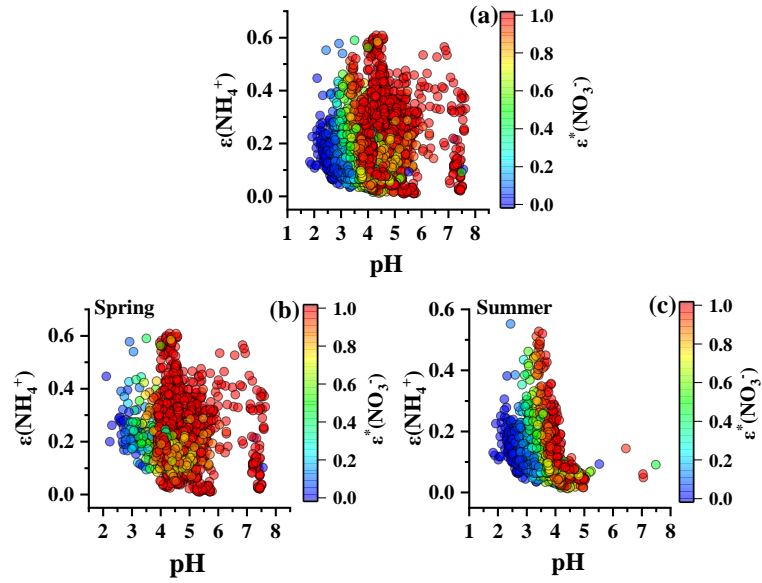


Fig. S7. $\epsilon(\text{NH}_4^+)$ as a function of pH for (a) all samples, (b) samples in spring, (c) samples in summer. Colors corresponds to theoretical $\epsilon(\text{NO}_3^-)$ ($\epsilon^*(\text{NO}_3^-)$)

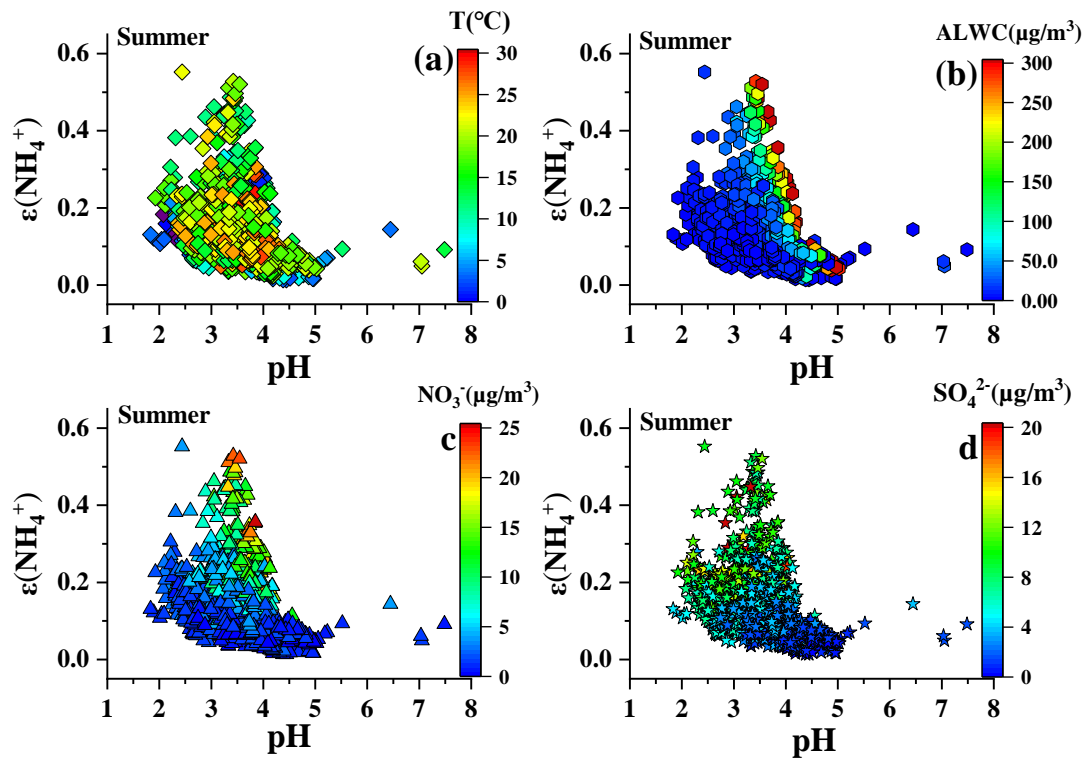


Fig. S8. $\epsilon(\text{NO}_3^-)$ as a function of pH for summer samples. The color of circles corresponds to (a) temperature, (b) ALWC, (c) observed NO_3^- , (d) observed SO_4^{2-}

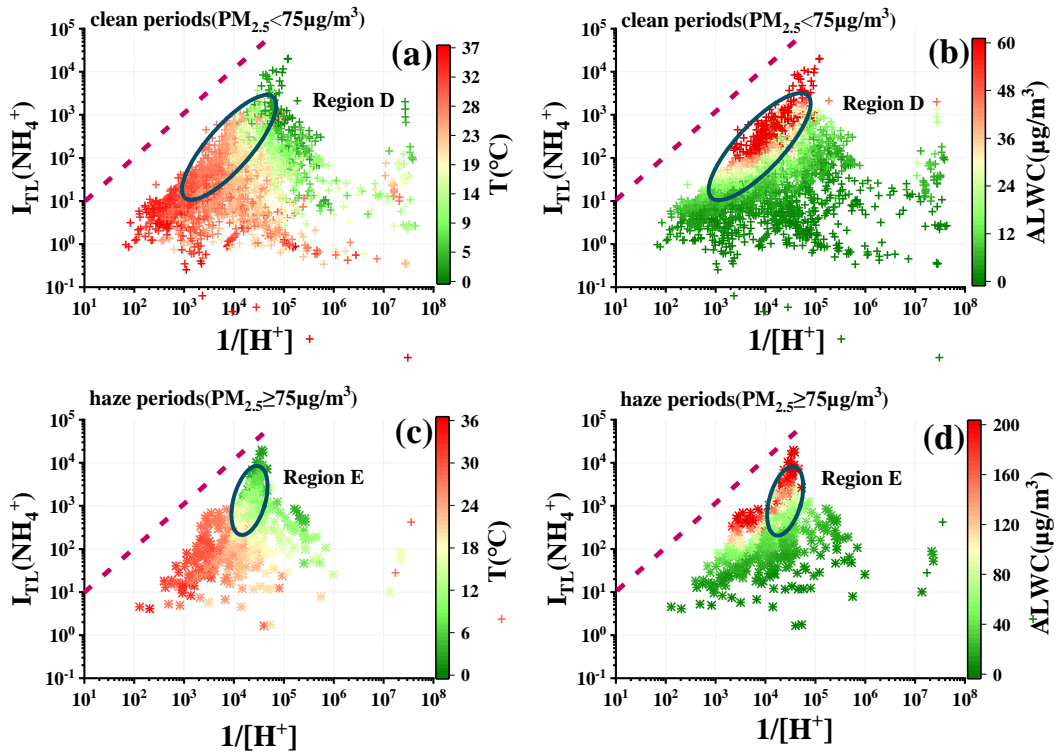


Fig. S9. The relationship between $I_{TL}(\text{NH}_4^+)$ and $1/[\text{H}^+]$ in $\epsilon(\text{NH}_4^+)$. Color represents temperature (a for clean periods, c for haze periods) and liquid water content (b for clean periods, d for haze periods)

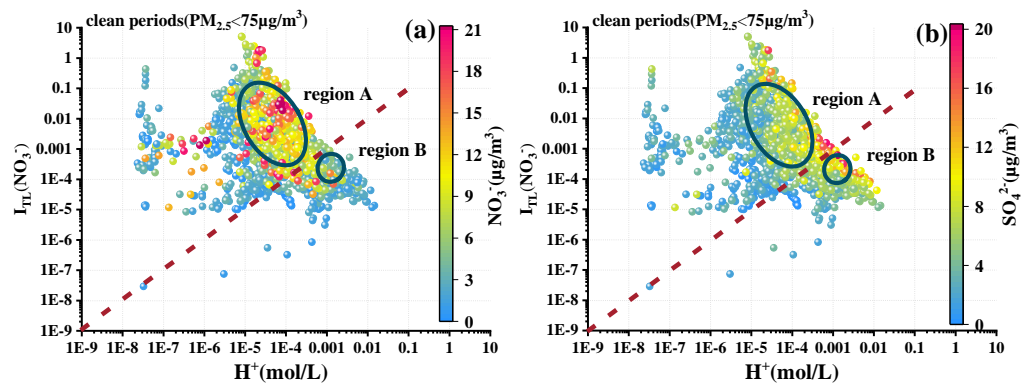


Fig. S10. The relationship between $I_{TL}(\text{NO}_3^-)$ and $[\text{H}^+]$ in $\epsilon(\text{NO}_3^-)$. Color represents observed concentrations of (a) NO_3^- , and (b) SO_4^{2-}

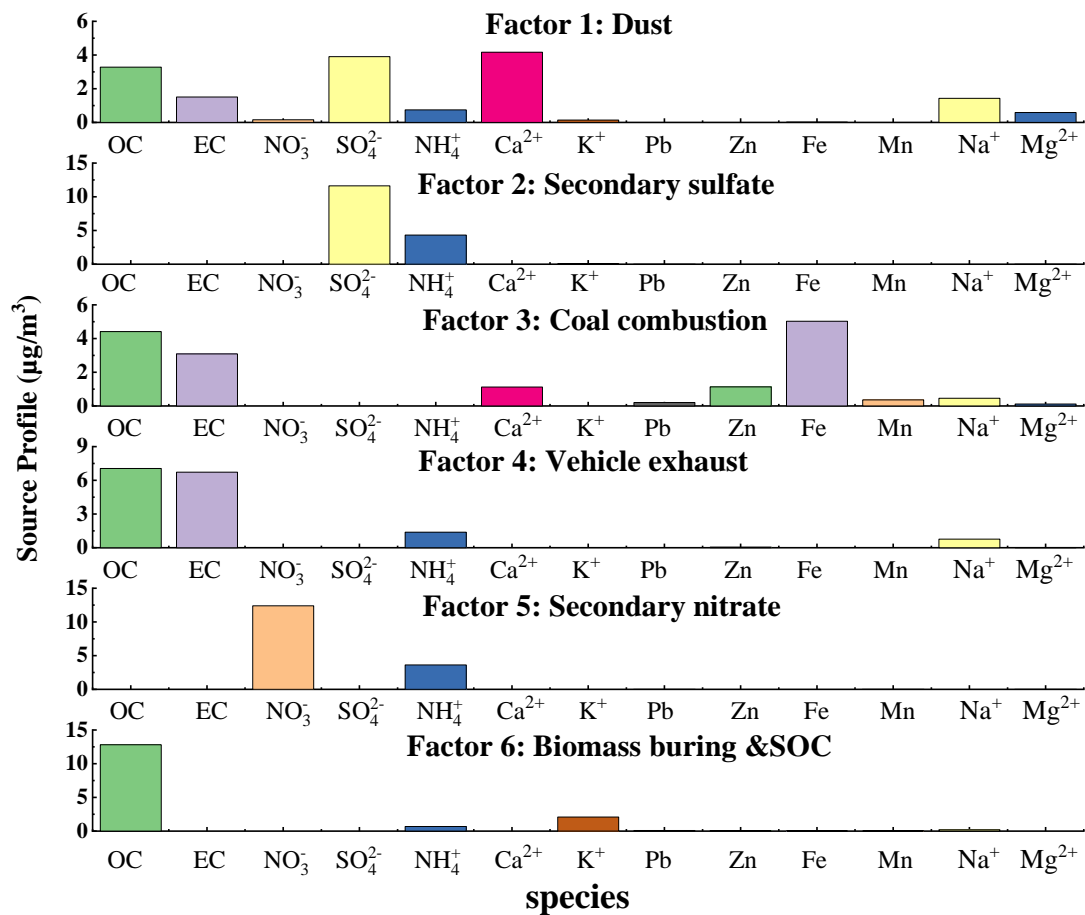


Fig. S11. The result of source apportionment

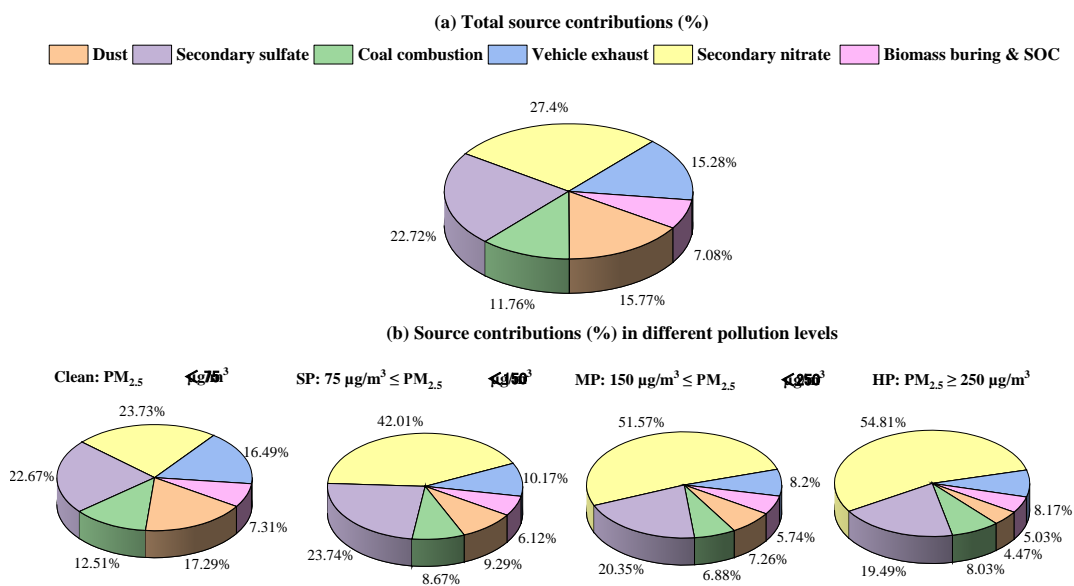


Fig. S12. Source contributions (a) over the entire sampling period, (b) among different pollution levels

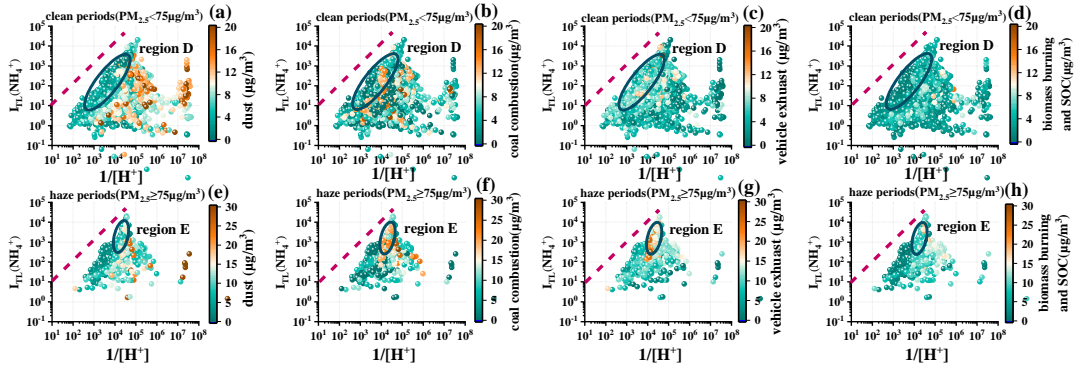


Fig. S13. The relationship between $I_{TL}(NH_4^+)$ and $1/[H^+]$ in $\epsilon(NH_4^+)$. Color represent contributions of dust (a, e), coal combustion (b, f), vehicle (c, g), and biomass burning and SOC (d, h) during clean periods (a through d), and haze periods (e through h)

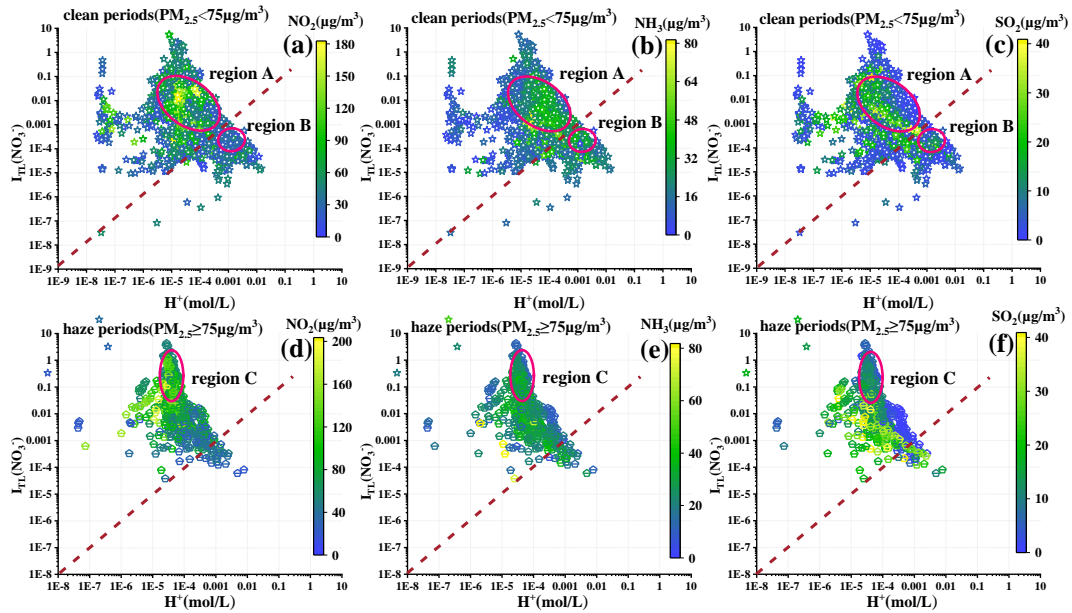


Fig. S14. $\epsilon(NO_3^-)$ as a function of pH for samples during clean and haze periods. Color of circles represent observed concentration of NO_2 (a, d), NH_3 (b, e), and SO_2 (c, f), during clean (a through c) and haze periods (d through f)

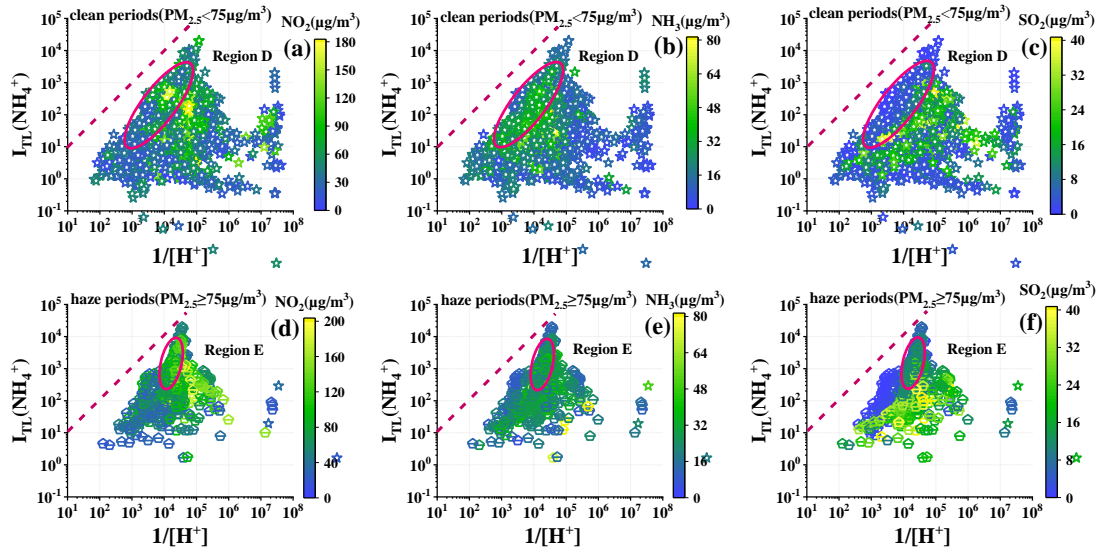


Fig. S15. $\varepsilon(\text{NH}_4^+)$ as a function of pH for samples during clean periods and haze periods.

Color of circles represent observed concentration of NO_2 (a, d), NH_3 (b, e), and SO_2 (c, f), during clean (a through c) and haze periods (d through f)

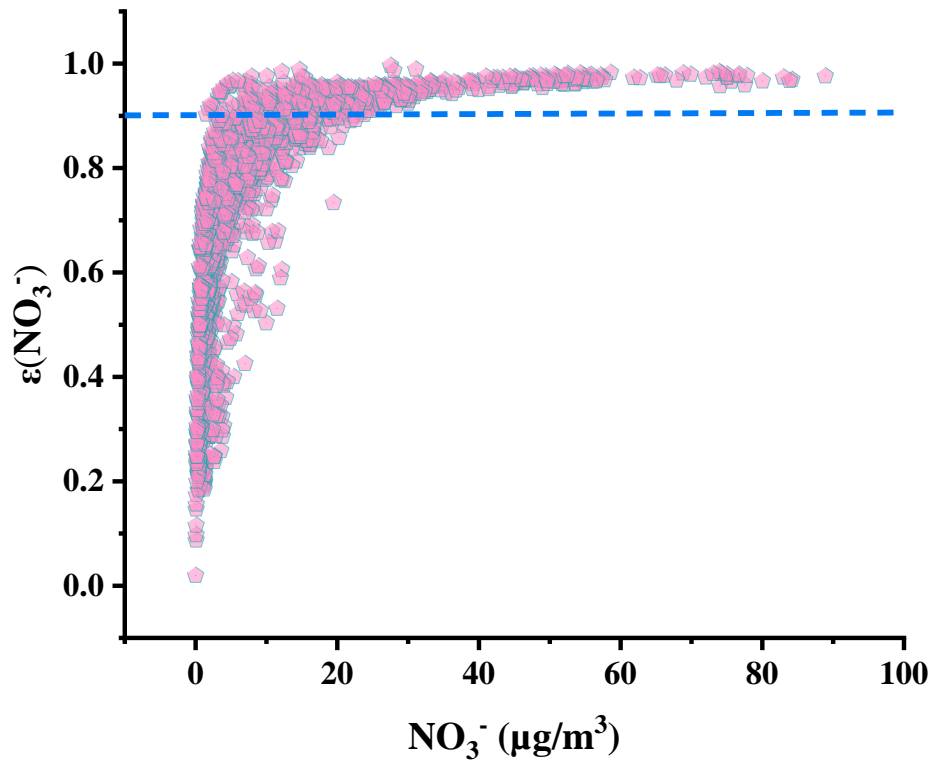


Fig. S16. The relationship between $\varepsilon(\text{NO}_3^-)$ and nitrate load in actual environmental atmosphere.

Table S1. Descriptive statistics of species and parameters during the entire sampling period and among different pollution levels.

Species/Parameters	Average ($\mu\text{g m}^{-3}$, except T, RH and pH)	Clean	Slightly polluted (SP)	Moderately polluted (MP)	Heavily polluted (HP)
PM _{2.5}	48.77	32.29	100.42	188.69	287.51
OC	4.56	3.86	6.74	10.47	14.99
EC	2.19	1.76	3.46	6.42	7.88
Cl ⁻	1.21	0.86	2.38	3.93	5.1
NO ₃ ⁻	9.08	5.11	19.78	47.69	76.6
SO ₄ ²⁻	6.04	4.65	10.37	17.97	25.7
NH ₄ ⁺	6.17	4.42	11.98	20.27	28.51
Na ⁺	0.51	0.49	0.54	0.71	0.85
K ⁺	0.27	0.21	0.46	0.77	0.94
Ca ²⁺	0.77	0.68	1.05	1.74	1.53
Mg ²⁺	0.11	0.1	0.13	0.22	0.23
SO ₂	7.83	6.9	11.31	15.26	12.73
NO ₂	53.34	49.08	67.99	87.96	98.57
NH ₃	23.84	22.88	28.24	28.87	25.04
O ₃	56.33	58.59	45.54	43.08	66.32
T (°C)	21.77	22.45	20.16	13.73	13.37
RH (%)	63.77	62.81	67.81	70.61	63.31
pH	4.13	4.12	4.17	4.37	4.25